RSC Advances

PAPER

View Article Online
View Journal | View Issue

Cite this: *RSC Adv.*, 2020, **10**, 42688

Removal of As^{3+}, As^{5+}, Sb^{3+}, and Hg^{2+} ions from aqueous solutions by pure and co-precipitated akaganeite nanoparticles: adsorption kinetics studies†

Verónica Villacorta, *[a] César Augusto Barrero, [a] María-Belén Turrión, [b] Francisco Lafuente,[b] Jean-Marc Greneche [c] and Karen Edilma García [a]

Adsorption kinetics models have been used to evaluate the adsorption behaviour of pollutants on different materials but there are no reports for the adsorption of As^{5+}, As^{3+}, Sb^{3+} and Hg^{2+} on co-precipitated akaganeite nanoparticles which were previously formed in the presence of these ions. In this research, the performance of pure and co-precipitated akaganeite nanoparticles as adsorbents of As^{3+}, As^{5+}, Sb^{3+} and Hg^{2+} in aqueous solutions was evaluated using the nonlinear kinetics models of Langmuir, Lagergren, Ho–McKay, Bangham, Elovich and simplified Elovich. In addition, transmission ^{57}Fe Mössbauer spectrometry was used for the first time to compare the physico-chemical properties of akaganeite before and after the adsorption processes. The results showed that co-precipitated akaganeites had much better adsorption capacities than pure akaganeites. On the other hand, the Sb^{3+} and Hg^{2+} were the fastest and slowest pollutants respectively adsorbed on all akaganeites. The kinetics models that best described the experimental data for As^{3+}, As^{5+} and Sb^{3+} were those of Elovich and simplified Elovich. For Hg^{2+}, the kinetic model that best described the experimental data was that of Bangham. The 300 K and 77 K Mössbauer spectrometry showed only slight variations in some of the hyperfine parameters for the akaganeites after adsorption.

Received 21st September 2020
Accepted 3rd November 2020

DOI: 10.1039/d0ra08075f

rsc.li/rsc-advances

1 Introduction

Akaganeite, the β polymorph of FeOOH, is a natural product of iron corrosion in chloride-containing environments.[1,2] This oxyhydroxide has been widely used as a precursor to hematite and other magnetic recording materials[3,4] and in the electrocatalysis, pigment, ion-exchange and semiconductor applications.[3,5] Furthermore, due to its availability, low cost, large specific surface area, the presence of tunnel sites and the numerous possibilities of synthesis with modified surfaces, akaganeite has been employed as an adsorbent for removing toxic ions such as Zn^{2+}, Pb^{2+}, Cd^{2+}, Cr^{6+}, As^{3+}/As^{5+}, Sb^{5+}, U^{6+}, and antimony and arsenic methylated species from polluted water and nuclear waste streams. In this regard, Guo and co-workers,[6] compared the affinity of Sb^{3+} and Sb^{5+} for akaganeite. To this end, the authors carried up adsorption experiments at different pH values, for 24 h at 25 °C. The authors reported that the adsorption of Sb^{3+} was constant over a broad pH range, while the Sb^{5+} adsorption was favored under acidic conditions. Zhang and Jia,[7] synthesized ultra-small and well dispersed akaganeite nanorods and then used them to adsorb As^{5+}. In their kinetic study, the initial As^{5+} concentrations were 5.20 ppm and the adsorbent dose was 1.0 g L^{-1}. In addition, the suspension was placed into an air incubator at an agitation speed of 150 rpm at 25 °C and a pH of 7.20. The results showed that the adsorption data were well fitted to a pseudo second-order kinetic model. Furthermore, the adsorption rate toward As^{5+} was very fast, such that most of As^{5+} could be removed after 1 h. In order to reveal the adsorption mechanism, the authors analysed before and after the adsorbents by FTIR and XPS, and observed that after adsorption the band at 847 cm^{-1} (assigned to the in-plane bending vibrations of hydroxyl groups of O–H···OH_2 and O–H···Cl hydrogen bonds) was turned weak, and at the same time, a new band at 814 cm^{-1} was observed. The new band was attributed to As–O vibration of As^{5+} suggesting the ion-exchange between the hydroxyl groups bonded to the water molecules outside of the tunnels and As^{5+}. Kolbe and co-workers,[8] concluded that the best results for the removal of antimonate and arsenate onto akaganeite were achieved under acidic

[a]Solid State Group, Faculty of Exact and Natural Sciences, University of Antioquia – UdeA, Street 67 N° 53-108, Medellín, Colombia. E-mail: vvillacortal@unal.edu.co

[b]Institute on Sustainable Forest Management, Department of Agroforestry Sciences, Area of Soil Science and Agricultural Chemistry, University of Valladolid, Palencia, Spain

[c]Institut des Molécules et Matériaux du Mans – IMMM UMR CNRS 6283, Université du Maine, Le Mans, Cedex 9, 72085, France

† Electronic supplementary information (ESI) available. See DOI: 10.1039/d0ra08075f

conditions, while the sorption of arsenite had an optimum at pH 7. The maximum loadings varied from 450 mg g^{-1} (antimonate at pH 2.2) to 2 mg g^{-1} (trimethyl antimonate at pH 7). Yusan and Erenturk,[9] applied the isothermal and kinetics models to explain the U^{6+} adsorption on akaganeite. Three kinetics models were used to fit the adsorption kinetics data: the pseudo first-order or Lagergren, the pseudo second-order or Ho and McKay and the Morris–Weber intraparticle diffusion models. Kinetics evaluation data showed that the adsorption of U^{6+} on akaganeite followed well the pseudo second-order kinetic model, highlighting chemical sorption as a step limiting the velocity of adsorption mechanism. Moreover, the authors concluded that the intraparticle diffusion was also the rate-limiting step. Deliyanni and co-workers,[10] investigated the zinc removal from aqueous solution by sorption on a nanocrystalline akaganeite. The authors used kinetics models in order to study the mechanism of sorption and potential rate control step. They also observed a complete removal of Zn^{2+} (10 ppm) at 20 h, pH 6.5 and 25 °C with 1 g L^{-1} akaganeite concentration. Moreover, the best fit with the experimental data was achieved by application of Elovich's nonlinear kinetic model. Lazaridis and co-workers,[11] used nanosized akaganeite to the removal of hexavalent chromium from aqueous solutions. The authors defined the akaganeite sorption capacity from sorption equilibria and sorption kinetics. For the reaction kinetics, the researchers used the pseudo first-order, pseudo second-order and Crank nonlinear adsorption models. Inspection of the regression analysis revealed that intraparticle model yielded a better sum of squares of the residuals than the two reaction kinetics models, and that the second-order kinetic model was superior to the first-order model. They observed a sorption capacity of approximately 9 mg L^{-1} with akaganeite and Cr^{6+} concentrations of 1 g L^{-1} and 10 g L^{-1}, respectively, at 25 °C, pH 6.5 and at 250 minutes. Deliyanni and Matis,[12] examined the application of akaganeite for removal of cadmium ions from aqueous solutions through Langmuir and Freundlich sorption isotherms. The evidences obtained by the authors lead to a mechanism of weak chemisorption, which was well modelled by both models.

On the other hand, surface-modified akaganeites have shown great potential for environmental applications.[13] In this respect, Deliyanni *et al.*[14] developed an adsorbent based on a nanocrystalline–akaganeite hybrid surfactant, which was synthesized using a cationic surfactant, hexadecyltrimethylammonium bromide, as a modifier. The samples showed a significantly higher adsorption capacity for arsenate than for pure nanocrystalline akaganeite, as well as fast kinetics, which follows a pseudo second-order rate equation. Moreover, the authors observed that adsorption data could not be fitted to the Langmuir equation due to the heterogeneity of the sorbent surface following the modification. Tufo and co-workers,[15] studied the adsorption properties of As^{5+} on Al for Fe substituted akaganeites. The results indicated that Al-substitution enhanced the reactivity of the surface akaganeites towards As-adsorption. Sun and co-workers,[16] reported that Zr^{4+} substituted akaganeites had better adsorption capacities for As^{3+} and As^{5+} than pure akaganeites. Harijan and Chandra,[17] developed akaganeite nanorods and akaganeite nanorods decorated with graphene oxide sheets at 5%, 10% and 15% for adsorption of phosphate ions from water at pH 7. The FTIR spectra of β-FeOOH nanorods/graphene oxide showed peaks corresponding to akaganeite and a low intense peak corresponding to graphene oxide. When the authors compared the samples after and before of the phosphate adsorption by this technique, they found additional bands corresponding to the P–O stretching vibration in the HPO_4^{2-} groups. On the other hand, the adsorption experiments showed the maximum removal capacity for an adsorbent dose of 0.4 g L^{-1}, an initial phosphate concentration of 20 ppm, a time of adsorption of 2 h and a temperature of 30 °C. Under these conditions the maximum removal capacity followed the next order: β-FeOOH nanorods/graphene oxide at 5% > β-FeOOH nanorods/graphene oxide at 10% > β-FeOOH > β-FeOOH nanorods/graphene oxide at 15% > graphene oxide. Deliyanni and co-workers,[18] prepared and characterized an akaganeite modified with a cationic surfactant. The material was then used as an adsorbent to remove arsenite ions from aqueous solutions. The surfactant modified akaganeite had a much higher arsenite adsorption capacity than the pure akaganeite, which could be attributed to the presence of the surfactant. The kinetics adsorption follows a second-order rate equation and the isothermal sorption the Langmuir and Freundlich models. The maximum adsorption capacity obtained was found between 98 and 100% at pH 7, 25 °C, an adsorbent dose of 1 g L^{-1}, an adsorbate concentration of 10 mg L^{-1} and 24 h. The authors concluded that arsenite ions reacted with surface OH^- functional groups suggesting that specific adsorption occurred. The same authors observed that the maximum adsorption capacity for pure akaganeite under the same conditions was 135.2 mg g^{-1}. Finally, Deliyanni *et al.*[19] synthetized hybrid surfactant akaganeite nanoparticles which showed an efficiency of removal of As^{3+} from aqueous solution of 100–120 mg g^{-1} at pH 7.5, 25 °C and a contact time of 2 hours.

According to the bibliography reviewed, most authors have studied the phenomenon of pollutant adsorption on pure akaganeite but only a few on surface-modified akaganeites. We noted that modifying the surface properties of the akaganeites is a good strategy to improve their adsorption properties. One way to do this is to add surfactants and another is to prepare the samples in the presence of different types of cations. We mentioned above that, in the second case, there are reports of akaganeites prepared in the presence of Al^{3+} and Zr^{4+} ions. To the best of our knowledge, there are no reports on the use of akaganeite to adsorb Hg^{2+}. Moreover, there are no studies on the adsorption of Sb^{3+}, As^{5+}, and As^{3+} on modified akaganeites previously co-precipitated in the presence of these ions. In addition, most of the reported works use the isothermal models to define the sorption capacity of akaganeite and for a small number of them, the kinetics models.

In the present study, pure and co-precipitated akaganeites (in the presence of mercury, arsenic and antimony) were used as adsorbents of Sb^{3+}, As^{5+}, As^{3+} and Hg^{2+} in aqueous solutions. To understand the adsorption phenomena, we adjust the experimental data to different nonlinear kinetics models. Moreover,

the solid samples before and after adsorption were characterized by ^{57}Fe Mössbauer spectrometry at 300 and 77 K. The results showed that the co-precipitated akaganeites had much better adsorption capacities than pure akaganeites, as well as a faster initial average adsorption velocity. The kinetics models that best described the experimental data for As^{3+}, As^{5+} and Sb^{3+} adsorbates onto the adsorbents were Elovich and simplified Elovich. In the case of Hg^{2+} adsorbate was the Bangham nonlinear kinetic model. Mössbauer spectrometry showed slight variations in some of the hyperfine parameters for the akaganeites after adsorption compared to the parameters for the akaganeites before adsorption.

2 Materials and methods

2.1 Adsorbents preparation

Pure and co-precipitated akaganeites were synthesized from 0.05 M $FeCl_3 \cdot 6H_2O$ solutions (Merck, EMSURE®, ACS, Reag. Ph Eur.) in the absence and presence of dilute solutions of Hg^{2+}, Sb^{3+} and As^{5+} ions at 60 ppm, as described in Villacorta and co-workers.[20] The dilute solutions were prepared from standard solutions of $Hg(NO_3)_2$, 1000 ppm Hg in 2 M HNO_3 (Merck Certipur®), Sb_2O_3, 1000 ppm Sb in 2 M HCl (Merck Certipur®), and H_3AsO_4, 1000 ppm As in 0.5 M HNO_3 (Merck Certipur®). It is important to mention that the samples were code-named as follows: pAk for pure akaganeite; and Ak60Hg, Ak60Sb and Ak60As for akaganeites co-precipitated with 60 ppm Hg^{2+}, 60 ppm Sb^{3+} and 60 ppm As^{5+}, respectively.

2.2 Physico-chemical characterization of the adsorbents

Pure and co-precipitated akaganeites, prior to adsorption experiments, were characterized by using X-ray diffraction (XRD), high-resolution transmission electron microscopy (TEM) and Raman, IR and Mössbauer spectroscopies. The results obtained by XRD showed that the patterns of co-precipitated samples were similar to that of pure akaganeite, implying that this was the only compound precipitated in all experiments. It is important to highlight that Hg^{2+}, Sb^{3+} and As^{5+} did not replace Fe^{3+} at its crystallographic site, but the pollutants were located at both tunnels and surfaces of akaganeite during the nucleation and growth of the particles. All samples exhibited an acicular morphology, with average particle lengths of 503 ± 39, 29 ± 11, 23 ± 6 and 13 ± 3 nm, and with average particle widths of 107 ± 12, 9 ± 3, 6 ± 2 and 4 ± 1 nm, for pAk, Ak60Hg, Ak60Sb and Ak60As, respectively. From these results, it can be noticed that the pollutants induced dramatic reductions in the particle sizes, and also changed the morphology from nanostructured to nanoparticulated. Now, in order to determine the specific surface area (SSA) of the akaganeites was assumed as a good approximation that the particles exhibit a cylindrical shape. In this way, the SSA can be calculated trough the following equation:

$$\mathrm{SSA} = \left[\frac{A}{\rho V} = \frac{2(h+r)}{\rho r h}\right] \quad (1)$$

where A is the area of an akaganeite particle with cylindric form (m^2), ρ is the density of akaganeite (3.52 g cm^{-3}) and V is the volume of a cylinder (m^3). The height, h, and half-width, r, of the particles were obtained through the characterization of the adsorbents by TEM.[20] By using this equation, it was found that the SSA values for pAk, Ak60Hg, Ak60Sb and Ak60As, were of about 12, 209, 214, and 328 m^2 g^{-1}, respectively. These results imply that the specific surface areas of the co-precipitated akageneites are much larger than that of the pure akaganeite. Finally, important changes in the spectroscopic signals and Mössbauer hyperfine parameters were also obtained by the different techniques. More details of these analysis can be consulted in ref. 20.

2.3 Kinetics of adsorption

To carry out the adsorption kinetics, solutions of 200 mL at 40 ppm of: (i) As^{3+} 1000 ppm in NaOH 0.5%, NaCl 0.1% (Merck Certipur); (ii) H_3AsO_4 in HNO_3 0.5 M 1000 ppm As (Merck Certipur®); (iii) Sb_2O_3 in HCl 2 M 1000 ppm Sb (Merck Certipur®); and (iv) $Hg(NO_3)_2$ in HNO_3 2 M 1000 ppm Hg (Merck Certipur®), have been brought in contact with 100 mg of pure and co-precipitated akaganeites. Here, visual MINTEQ,[21] which is a free software used for solving many kinds of chemical equilibrium problems, was used with the objective to determine the predominant chemical species of Hg^{2+}, As^{5+}, As^{3+} and Sb^{3+} formed in the solutions at the actual conditions of adsorption experiments. The values used to perform the simulations were pH: fixed at 2; components names: Hg^{2+}, As^{5+}, As^{3+} and Sb^{3+}, concentration: 40 mg L^{-1}, temperature: 25 °C and ionic strength: to be calculated.

The suspensions were then stirred for 60 minutes at 300 rpm, so that at 1, 3, 6, 9, 12, 20, 40 and 60 minutes, 5 mL aliquots were taken and filtered with a 0.45 μm membrane disc; subsequently, the concentrations of As^{3+}, As^{5+}, Sb^{3+} and Hg^{2+} in the aliquots were analyzed by inductively coupled plasma-optical emission spectrometry (ICP-OES) using a Varian 725-ES apparatus.

The temperature of the experiments was controlled at 25 °C, while the pH was about 2. Kolbe and co-workers,[8] reported that the best results for the removal of antimonate and arsenate onto akaganeite were achieved under acidic conditions. On the other hand, in the case of acid mine drainage, whose pH can be 2, these pollutants are present, and in nature, mineraloids are the most efficient materials in their decontamination.[22]

The amount of metal ion adsorbed on the pure and co-precipitated akaganeites at time t, was given by the following equation:

$$Q_t = \left[\frac{(C_0 - C_t)V}{M}\right] \quad (2)$$

where Q_t is the adsorption capacity at specified time, t, (mg of pollutant adsorbed g^{-1} of adsorbent), C_0 is the initial concentration of pollutant in aqueous solution (mg L^{-1}), C_t is the pollutant concentration at time t (mg L^{-1}), V is the volume of metal ion solution (L) and finally M is the mass of sorbent (g).

Finally, for the adsorption kinetics, the samples were code-named as follows: pAk-Hg, pAk-Sb and pAk-As^{3+} for pure akaganeites adsorbing Hg^{2+}, Sb^{3+} and As^{3+} pollutants, respectively. Ak60Hg–Hg, Ak60Hg–Sb, Ak60Hg–As^{3+} and Ak60Hg–As^{5+} for Ak60Hg samples adsorbing Hg^{2+}, Sb^{3+}, As^{3+} and As^{5+} pollutants, respectively. Ak60Sb–Hg, Ak60Sb–Sb, Ak60Sb–As^{3+} and Ak60Sb–As^{5+} for Ak60Sb samples adsorbing Hg^{2+}, Sb^{3+}, As^{3+} and As^{5+} pollutants, respectively. And, finally, Ak60As–Hg, Ak60As–Sb, Ak60As–As^{3+} and Ak60As–As^{5+} for Ak60As samples adsorbing Hg^{2+}, Sb^{3+}, As^{3+} and As^{5+} pollutants, respectively.

The experimental data were fitted to the nonlinear kinetics models of Langmuir, Lagergren or pseudo order 1, Bangham, Ho and McKay or pseudo order 2, simplified Elovich and Elovich, with the objective of deciding which model (or models) best describe(s) the data. The equations corresponding to these models are showed in Table S1.†

2.3.1 Statistical analysis for kinetics models. This study used the software of origin program to adjust the experimental data obtained from kinetic experiments to Langmuir, Lagergren, Bangham, Ho and McKay, Elovich and simplified Elovich nonlinear kinetics models. All the range of experimental data as well as the dispersion of the same was considered to carry out the adjustments in each of the times. In order to evaluate the error of the models, the root of the mean square error (E) was used; likewise, the 95% confidence and prediction bands were taken into account. Only those models whose parameters presented convergence with a p-value less than 0.05 were recorded. Subsequently, only those statistically consistent models were graphed.

2.4 Physico-chemical characterization of solids obtained after adsorption

The different akaganeites with adsorbed pollutants were characterized by Mössbauer spectrometry.

2.4.1 ^{57}Fe Mössbauer spectrometry. The transmission Mössbauer spectra for all samples were recorded at 300 K and 77 K using a source of 25 mCi ^{57}Co diffused in a Rh matrix. Mössbauer spectra were collected in a time-mode spectrometer working in the transmission geometry using a constant acceleration drive with triangular reference signal. Calibration was achieved from standard α-iron foil at 300 K. The spectra were analyzed using a home-made program called MOSFIT which is based on nonlinear least squares fitting procedure assuming Lorentzian Mössbauer lines while the values of isomer shift are quoted to that of α –Fe at 300 K.

3 Results and discussion

Regarding the synthesis of akaganeites in the presence of Hg^{2+}, As^{5+}, and Sb^{3+}, it was reported that these pollutants induced changes in the unit cell parameters, the mean crystallite size, the activation energies for akaganeite nucleation and growth and in some vibrational modes.[20] All changes were in well agreement with the hypotheses that the pollutants were adsorbed at the surface and in the case of As^{5+} also at tunnel sites. The average crystallite size determined by Rietveld analysis of the XRD patterns was of 134 ± 19 nm for pure akaganeite (pAk) and of 20 ± 1, 17 ± 1 and 13 ± 1 nm, for Ak60Hg, Ak60Sb and Ak60As, respectively.[20]

In all adsorption kinetics experiments, the pH values were approximately 2 for adsorbing Hg^{2+}, As^{5+}/As^{3+} and Sb^{3+}. Using the MINTEQ software,[21] and considering the pH values of our experiments, we determined that the predominant chemical forms of Hg^{2+}, As^{5+}, As^{3+} and Sb^{3+} were: Hg^{2+} with a total concentration of 96.5%, H_3AsO_4 and $H_2AsO_4^-$ with a total concentration of 64.8 and 35.2%, respectively, H_3AsO_3 with a total concentration of 100%, and finally, $Sb(OH)_2^+$ and $Sb(OH)_3$ with a total concentration of 20.6 and 79.4%, respectively. These results are consistent with those reported in the literature.[23]

3.1 Adsorption kinetics

Fig. 1 show the adsorption kinetics of Hg^{2+}, Sb^{3+}, As^{5+} and As^{3+} on pure and co-precipitated akaganeites. The adsorption kinetics of As^{5+} on Ak60Hg were complicated to obtain due to formation of toxic vapours, and therefore are not included.

In the construction of the adsorption kinetics for Sb^{3+} and Hg^{2+}, the three points of the same colour corresponded to Q values collected at the same time and for three different wavelengths of the ICP-OES equipment. In the case of antimony, the readings were at 206.834, 217.582, and 231.146 nm, while mercury at 184.887, 194.164, and 253.652 nm. On the other hand, for As^{3+} and As^{5+}, the Q data at a given time were collected with four different wavelengths corresponding to four readings at 188.980, 193.696, 197.198 and 234.984 nm.

Now, from Fig. 1, it can be seen that the Q values at 40 and 60 minutes are very similar for co-precipitated samples adsorbing Hg^{2+}. This result could indicate that at 60 minutes the experimental maximum adsorption capacity was probably reached. This situation was different for the co-precipitated samples adsorbing As^{3+}, As^{5+} and Sb^{3+} whose kinetics showed a slight continuous increase from 40 to 60 minutes. This result probably suggests the existence of a secondary reaction, surface precipitation or ternary adsorption, which can be seen as the formation of a new surface phase or as a multilayer adsorption due to the continuity of the process beyond adsorption.[24–27] In the case of arsenate and arsenite adsorption, it is important to stand out that in agreement with Cornell and Schwertmann,[28] the kinetics of adsorption on goethite and ferrihydrite seem to involve two stages: initial rapid adsorption followed by slower adsorption, whose data can be adjusted to the Elovich equation, as in this research was also observed.

For comparative purposes the experimental Q value at 60 minutes was correlated with experimental maximum adsorption capacity, Q_{max}. Table S2† lists the mean experimental Q_{max} for the different experiments at $t = 60$ min. Several interesting observations can be noted from these data. The co-precipitated akaganeites had higher adsorption capacities for the pollutants than pure akageneites. In fact, in the case of Hg^{2+}, As^{3+} and Sb^{3+}, the co-precipitated akaganeites adsorbed between 1.1 to 1.5, 1.4 to 1.8 and 2.2 to 2.6 times more than the pure akaganeite, respectively. This observation was perhaps due to the fact that

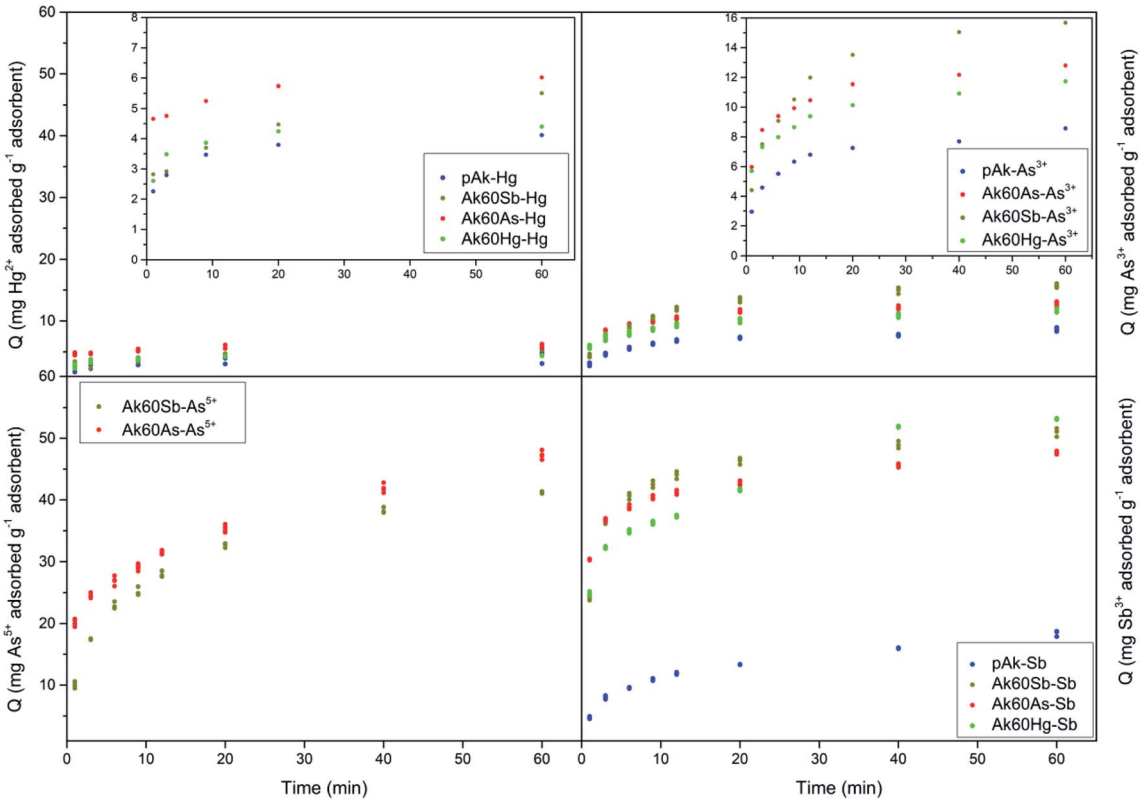

Fig. 1 Comparison of the adsorption capacity of Hg^{2+}, As^{3+}, As^{5+} and Sb^{3+} on the different adsorbents. Q (mg of pollutant adsorbed g^{-1} of adsorbent) is the adsorption capacity at specified time, t (min).

the co-precipitated samples had smaller mean particle sizes than pure akaganeite (134 ± 19, 20 ± 1, 17 ± 1 and 13 ± 1 nm for pure akaganeite, Ak60Hg, Ak60Sb and Ak60As, respectively).[20] Moreover, the higher adsorption capacity can also be due to the fact that the surface of the co-precipitated akaganeites presented a greater heterogeneity motivated by the presence of different active sites. This idea is in agreement with the structural changes observed in the co-precipitated samples compared with the pure sample due to the incorporation of the pollutants to the surface during the synthesis.[20]

On the other hand, Sb^{3+} was the best adsorbed pollutant by pure and co-precipitated akaganeites compared to the other contaminants, while Hg^{2+} was the least adsorbed one. In fact, the experimental maximum adsorption capacities of pollutants by co-precipitated akaganeites varied, from the highest to the lowest values, in the following order: $Sb^{3+} > As^{5+} > As^{3+} > Hg^{2+}$. A very interesting result is that the highest experimental Q_{max} values for a given pollutant were found to be independent of the type of co-precipitated akaganeite, *i.e.* the type of cation used to synthetized it, suggesting that for the adsorption experiments, the morphological properties of the samples are more important than the type of cations used to prepared it. This result is in good agreement with that reported by Tufo and co-workers,[15] who found that the morphological characteristics, in comparison with the Al^{3+} co-precipitated akaganeites, are the most important factors for the adsorption properties.

Now, in order to get an idea of the rate at which the pollutants are adsorbed by the adsorbents, we calculated the average sorption velocity, $\frac{\Delta Q}{\Delta t}$, in mg g^{-1} min^{-1}, for all samples from the experimental data, using the following equation:

$$\frac{\Delta Q}{\Delta t} = \frac{Q(t_{i+1}) - Q(t_i)}{t_{i+1} - t_i} \quad (3)$$

where t_i is the time for data i and $Q(t_i)$ is the adsorption at that time. The variations of $\frac{\Delta Q}{\Delta t}$ *versus* t_{i+1} for the full range of times are shown in Fig. 2. It can be seen that the mean adsorption velocity was very fast at the initial times, and from 3 minutes onwards it went to zero and remained in this value (see also zooms inside graphics of experimental mean sorption rate (mg g^{-1} min^{-1}) of adsorption of pollutants on akaganeites in the first 6 minutes of adsorption). For all akaganeites, the initial mean sorption velocities of pollutants, from the highest to the lowest, followed the order: $Sb^{3+} > As^{5+} > As^{3+} > Hg^{2+}$. These results mean that Sb^{3+} is the most rapidly adsorbed pollutant, while Hg^{2+} is the slowest adsorbed pollutant by all the akaganeites, in agreement with the order observed above for the maximum adsorption capacity of the pollutants, in which the antimony was the most adsorbed pollutant followed by As^{5+}, As^{3+} and Hg^{2+}.

3.2 Adsorption kinetics models

Our next step is to fit the experimental data with different kinetics models, to decide which model(s) correctly describe(s)

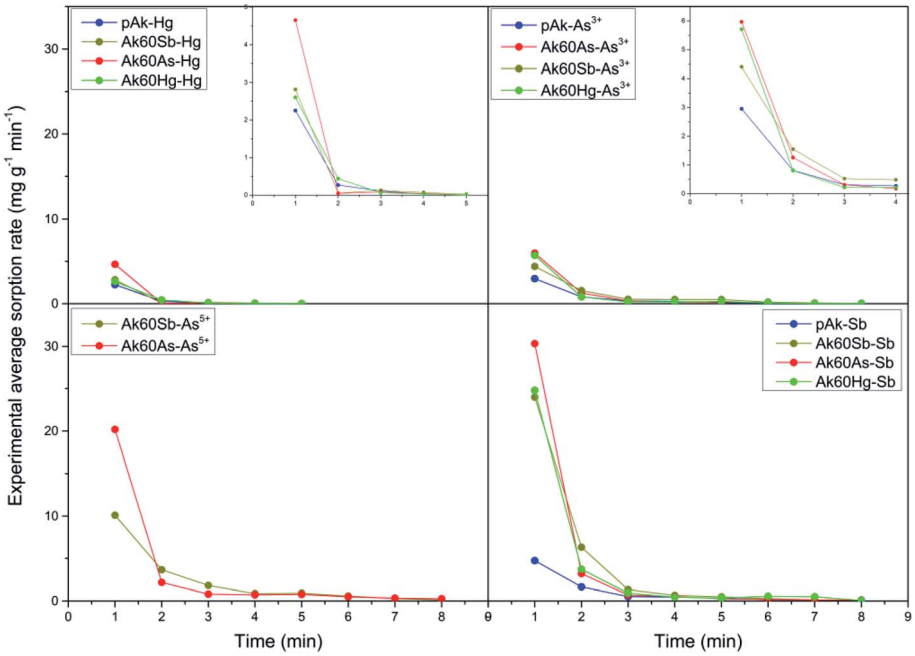

Fig. 2 Experimental mean sorption rate (mg g^{-1} min^{-1}) of adsorption of pollutants on akaganeites.

the data and to better understand the adsorption phenomena. In this study, six nonlinear adsorption kinetics models were used to fit the experimental data. Fig. 3–6 show the adjustment of the experimental data to the nonlinear adsorption kinetics models of Bangham, simplified Elovich and Elovich. The experimental data fit by Langmuir and Ho–McKay kinetics models did not show convergence, and in consequence are not shown here. On the other hand, the fits of the experimental data to the Lagergren model are not shown here because of the high root mean square errors. The values of parameters derived from the adjustments are listed in Table S3.†

In general, on the basis of a simple visual examination of Fig. 3–6, and on the *E* values reported in Table S3,† it can be seen that the experimental data are best described for Hg^{2+} by the Bangham nonlinear kinetic model, and for As^{3+}, As^{5+} and Sb^{3+} by Elovich and simplified Elovich nonlinear kinetics models.

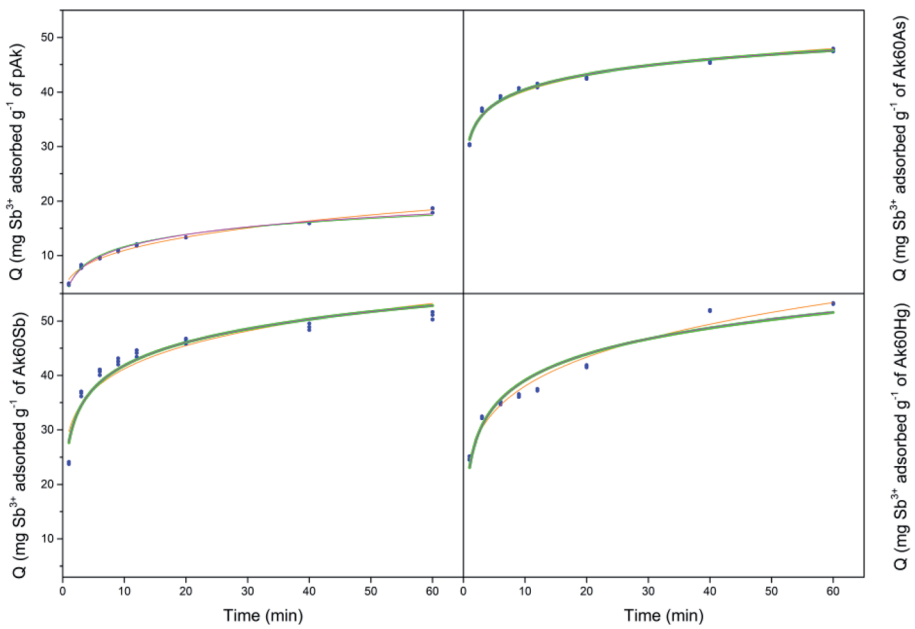

Fig. 3 Kinetics of adsorption of Sb^{3+} onto pAk, Ak60As, Ak60Sb and Ak60Hg. The experimental data (blue circles) are modelled with Bangham (orange), simplified Elovich (green) and Elovich (magenta) nonlinear models.

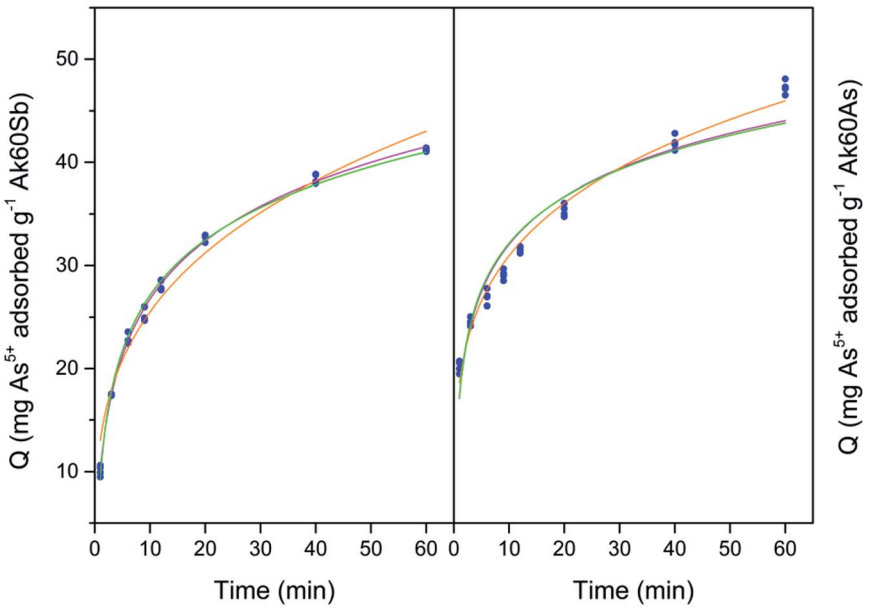

Fig. 4 Kinetics of adsorption of As^{5+} onto Ak60Sb and Ak60As. The experimental data (blue circles) are modelled with Bangham (orange), simplified Elovich (green) and Elovich (magenta) nonlinear models.

According to,[29] the Bangham model is an internal diffusion model, meaning that the slowest stage of adsorption refers to diffusion of the adsorbate to active sites located on the adsorbent surface. The values of Q_{max} obtained from the Bangham equation, 4.2, 4.6, 5.4 and 6.1 mg g^{-1} to pAk–Hg, Ak60Hg–Hg, Ak60Sb–Hg and Ak60As–Hg, respectively, were very close to those obtained from the experimental Hg adsorption data (see Table S2†).

On the other hand, for Sb^{3+}, As^{5+} and As^{3+} the Elovich and simplified Elovich models should be highlighted; indeed, in this case both models are adsorption models in which the slowest step of adsorption is the adsorption itself. In addition, chemisorption prevails over physisorption, and an energetic heterogeneity characterize the surface.[29] It is important to recall that α and β parameters refer respectively to the initial sorption rate and an energy activation constant for chemisorption. In Table S3,† it can be observed that the values of α (mg g^{-1} s^{-1})

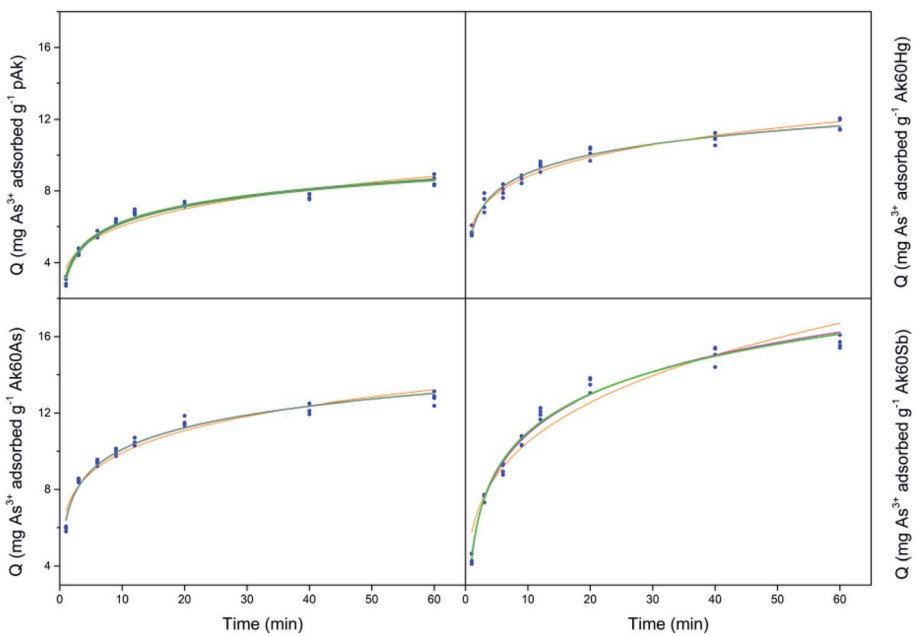

Fig. 5 Kinetics of adsorption of As^{3+} onto pAk, Ak60Hg, Ak60As, and Ak60Sb. The experimental data (blue circles) are modelled with Bangham (orange), simplified Elovich (green) and Elovich (magenta) nonlinear models.

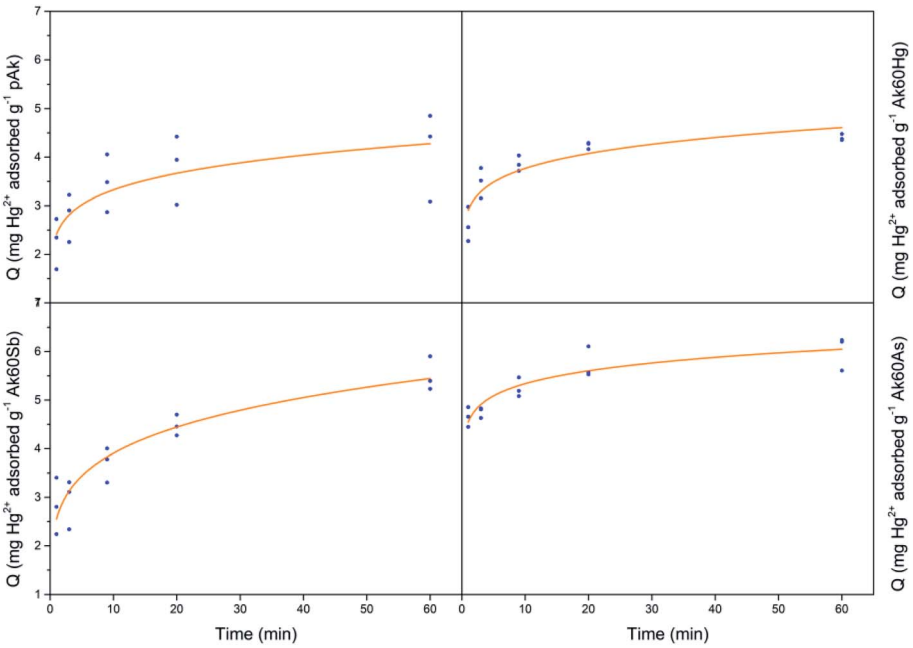

Fig. 6 Kinetics of adsorption of Hg^{2+} onto pAk, Ak60Hg, Ak60Sb, and Ak60As. The experimental data (blue circles) are modelled with Bangham (orange) nonlinear models.

increased for co-precipitated akaganeites adsorbing Sb^{3+}, As^{5+} and As^{3+} compared with the pure sample. These observations are in agreement with the experimental initial mean sorption rates for Sb^{3+}, As^{5+} and As^{3+} adsorption calculated by eqn (2) (see Fig. 2), which changed from the high to the low values in the following order $Sb^{3+} > As^{5+} > As^{3+}$; and with the observation that the Ak60As was the adsorbent on which all adsorbates were adsorbed the fastest during the first minutes (Fig. 2). Similarly, the values of β (g mg^{-1}) decreased in all cases compared with those of the pure sample.

The observations found in the evolution of α and β parameters indicated that As^{3+}, As^{5+} and Sb^{3+} probably accessed to the surface of co-precipitated akaganeites easier than to the surface of pure akaganeites, due to the increase of the α parameter and to the decrease of the β parameter compared with those of the pure sample. Some factors that probably influenced the values of α and β parameters are the mean particle size, that was lower for co-precipitated samples compared with pure akaganeite, the heterogeneity of the structure and the different surface active sites.

The agreement between the experimental data and the theoretical predictions based on the Elovich and simplified Elovich models confirms the heterogeneous sorption mechanism that could be responsible for the adsorption of As^{3+}, As^{5+}, and Sb^{3+} ions. This result is in agreement with the idea of the existence of different adsorption sites, which in the case of akaganeite would refer to tunnel sites and surface sites;[16] such as hydroxyl groups[28] and in our case the adsorbed As^{5+} and Sb^{3+} sites.

On the other hand, the incorporation of the adsorbed species depends fundamentally on the physicochemical characteristics of the adsorbent surface, such as the heterogeneity, specific surface area, the coordination sites, density and arrangement of the functional groups and the surface charge, among others.[26,28,30] Moreover, the ionic environment and pH of the solution in contact, the size and nature of adsorbate and the duration of the adsorption, also influence the adsorption process.[26,28,30] Here, it is important highlight the relation among the surface charge and the ionic species of the pollutants in solution. According to MINTEQ software, at pH 2 the predominant chemical forms of Hg^{2+}, As^{5+}, As^{3+} and Sb^{3+} are: Hg^{2+} with a total concentration of 96.5%, H_3AsO_4 and $H_2AsO_4^-$ with total concentrations of 64.8 and 35.2%, respectively, H_3AsO_3 with a total concentration of 100%, and finally, $Sb(OH)_2^+$ and $Sb(OH)_3$ with total concentrations of 20.6 and 79.4%, respectively. In agreement with Deliyanni and co-workers,[31] the pzc of akaganeite is approximately 7.3, so below this pH the surface of the akaganeite is positively charged. In this way, the adsorption of As^{5+} as $H_2AsO_4^-$ could be favoured. However, according with the results obtained in the adsorption kinetics models, the chemisorption prevailed over physisorption and in consequence the formation of internal sphere complexes probably changed the point zero charge since it involved the formation of specific chemical reactions between the surface and the adsorbates.

To complement this information, the free energy of adsorption can be defined as the sum between the chemical energy of adsorption and the electrostatic component: $\Delta G_{adsorption} = \Delta G_{chemical} + \Delta G_{coulombic}$.[28] In this way, when the affinity between the surface of the material and the ions present in the solution is very high, the chemical component of the adsorption energy predominates, and in consequence the generated bonds have a strong covalent character, causing internal sphere complexes. This situation originates that the

adsorption of neutral species or with the same charge of the surface can take place.[25,28,30]

Finally, the experimental data were less well adjusted to the Lagergren model, which is also an adsorption model where the slowest stage of the process is that of adsorption itself.[29] In this model, the saturated monolayer is considered as the maximum adsorption.[29] From this result, it could be thought that in adsorption of As^{3+}, As^{5+}, and Sb^{3+} a multilayer adsorption occurred, due to the loss of the plateau and to the increase of the adsorption (see Fig. 1).

3.3 ^{57}Fe Mössbauer spectrometry

In order to better understand the adsorption mechanism, we characterized the pure and co-precipitated akaganeites after the adsorption experiments and compared these results with the properties found for these akaganeites before the adsorption.[20] The results of the analysis of the akaganeites obtained after adsorption of pollutants through 300 and 77 K Mössbauer spectrometry are presented in Fig. S1–S6 and in Tables S4 and S5.†

Fig. S1–S3† show the 300 K Mössbauer spectra of samples pAk, Ak60Hg, Ak60Sb, and Ak60As after adsorption of Hg^{2+}, As^{3+} and Sb^{3+}. All spectra were first correctly fitted by introducing two quadrupolar doublets named D1 and D2 and the refined values of hyperfine parameters are listed in Table S4.† It is noted that, within the error bars, the hyperfine parameters (isomer shifts and quadrupole splittings) of the two ferric iron sites for all samples are quite similar. Now, samples pAk and pAk-As^{3+} showed similar relative spectral areas. On the contrary, the relative spectral areas of the two components for the samples Ak60Hg, Ak60Sb and Ak60As without and with adsorbed pollutants showed some differences. It is important to note that other fitting models can be considered assuming free values of linewidth and/or absorption areas, and/or some constraints: as the hyperfine structure of the quadrupolar spectra is poorly resolved, the main relevant hyperfine parameters are the mean values which are independent of the fitting models. As shown in Table S6,† the mean values of isomer shift and quadrupolar splitting are rather similar.

As shown in Fig. S4–S6,† all spectra obtained at 77 K exhibit rather similar complex hyperfine structures resulting from magnetic sextets composed of asymmetrical lines. The initial fitting procedure consists of four sextets named S1, S2, S3 and S4. These components arise from the existence of four non-equivalent iron sites related to the two monoclinic iron sites (Fe1 and Fe2) in the vicinity of occupied (Cl) or unoccupied (V_{Cl}) chloride sites.[20] Therefore, S1, S2, S3 and S4 are assigned to Fe1–Cl, Fe2–Cl, Fe1–V_{Cl} and Fe2–V_{Cl}, respectively. During fitting, the values of the isomer shift, quadrupolar shift, linewidth and absorption area for components S1 and S2 on the one hand, and those for components S3 and S4, on the other hand, can be constrained independently or not, either to be equal, or adjustable. In addition, the values of the hyperfine field were refined without constraint. Finally, many fitting models can be well realized with various sets of hyperfine parameters, leading to similar factors of goodness. At this stage, it remains difficult to establish which of these different models is the best solution. Table S5† shows an example of the values of the hyperfine parameters at 77 K characteristic of the samples pAk, Ak60Hg, Ak60Sb and Ak60As after adsorption of Hg^{2+}, As^{3+} and Sb^{3+}. Therefore, as in the case of quadrupolar doublets, we need to consider the mean values of each hyperfine parameter, including their respective error bars. They are also given in Table S7;† it is now difficult to establish some significant correlation between such these hyperfine parameters, the nature and content of contaminant, but they show unambiguously the presence of ferric species. The lack of strong evolution can be explained first of all by the low content of contaminant which must preferentially deform the superficial structure, causing thus a small effect.

The results found here suggest that in some cases the adsorption of pollutants by akaganeite slightly modifies certain hyperfine parameters. The isomer shift is the least sensitive parameter. To understand the Mössbauer results, it is worth discussing three aspects: first, how the atomic environment surrounding the Fe^{3+} ion and its molecular bonding with the ligands affect the hyperfine interactions; second, the relative abundance of iron ions at the surface of akaganeites; and third, the types and distribution of active sites for adsorption. With respect to the first aspect, the p–d electron population of the Fe ion affects the magnitude of the quadrupole shift and the hyperfine magnetic field. The population of this valence shell is affected by the molecular bonding of the iron with its neighbors. In akaganeite, Fe directly bonds to oxygen in the octahedral site. Oxygen share bonding with pollutants located at the surface and with hydrogen, which also bonds to chloride into tunnels and to pollutants at the surface. In summary, the slight variation in some of the hyperfine parameters could be partially explained by the fact that the adsorption of the pollutants at the surface and at tunnel sites, indirectly affects the Fe 3d orbital population. Now, with regard to the second aspect, the small variations in the hyperfine parameters can also be understood if we take into consideration that the adsorption process is mainly a superficial phenomenon, *i.e.* the pollutants are adsorbed at surface sites, and in the case of akaganeite, also tunnels can be also part of the adsorption sites. Here it is interesting to note that,[20] we studied the relative abundance of the surface iron ions with respect to the core irons for the different akaganeites. We found that for a shell thickness of $x = 0.2$ nm, the shell-volume to particle-volume ratio accounts for 1%, 10%, 14% and 22% for pAk, Ak60Hg, Ak60Sb and As60Ak, respectively. Thus, there are more irons located at the core than at the surface of the akaganeites, therefore explaining the very small variations observed in the hyperfine parameters. Finally, and concerning the third point, it is important to take into account that not all the surface sites available in akaganeite are active for adsorption. In this respect, Song and Boily,[32] theoretically and experimentally determined the identity and distribution of the adsorption sites at the surfaces of the akaganeite. They reported that reactions occurring on surfaces sites may involve hydroxyl, oxygen and water groups. In pure akaganeites, terminal (001) and (100) planes expose a mixture of the three types of hydroxyl groups (singly, doubly and triply coordinated to iron). On the

other hand, terminal (010) plane exposes a mixture of hydroxyl, oxygen and water groups. Not all of these sites are active for adsorption and their relative abundance is different.

4 Conclusions

In the present work, we have studied the adsorption kinetics of Sb^{3+}, As^{5+}, As^{3+} and Hg^{2+} ions in aqueous solutions onto pure and Hg^{2+}, As^{5+} and Sb^{3+} co-precipitated akaganeites through adjustment of the experimental data to different nonlinear kinetics models, as well as the characterization of solid samples before and after the adsorption. Carrying out this type of study is important because it generates information about the speciation and fate of this type of pollutants in aqueous environments. At the experimental conditions, and according to MINTEQ software, these ions were adsorbed under the following predominant chemical forms: H_3AsO_4 and $H_2AsO_4^-$ with total concentrations of 64.8 and 35.2%, respectively, H_3AsO_3 with a total concentration of 100%, Hg^{2+} with a total concentration of 96.5% and finally, $Sb(OH)_2^+$ and $Sb(OH)_3$ with total concentrations of 20.6 and 79.4%, respectively. We have found that the kinetics models that better described the adsorption experimental data for Sb^{3+}, As^{5+} and As^{3+} ions onto pure and co-precipitated akaganeites were Elovich and simplified Elovich nonlinear kinetics models; and for Hg^{2+} ion the Bangham model. In the case of Hg^{2+} adsorption, the rate-controlling mechanism of the adsorption process was probably the intraparticle diffusion, whereas in the case of Sb^{3+}, As^{3+}, As^{5+} adsorption, it was probably of chemical nature. The co-precipitated akaganeites had much better adsorption capacities than pure akaganeites. The maximum adsorption capacities of pollutants onto the co-precipitated akaganeites followed the order: $Sb^{3+} > As^{5+} > As^{3+} > Hg^{2+}$. The highest Q_{max} values for a given pollutant were found to be independent of the type of cation used to co-precipitate the akaganeite, suggesting that the morphological properties of akaganeites are important factors in determining their adsorption properties. Sb^{3+} was the most rapidly adsorbed pollutant, while Hg^{2+} was the slowest one. Finally, Mössbauer spectrometry showed small variations in some of the hyperfine parameters of akaganeite after adsorption of different pollutants in comparison to akaganeite before adsorption.

Conflicts of interest

There are no conflicts to declare.

Acknowledgements

The financial support from CODI-Universidad de Antioquia (Estrategia de Sostenibilidad del Grupo de Estado Sólido 2018–2019, ES84180123) is greatly acknowledged.

References

1 J. E. Post and V. F. Buchwald, Crystal structure refinement of akaganéite, *Am. Mineral.*, 1991, **76**, 272–788.
2 S. D. Yusan and S. Akyil, Sorption of uranium (VI) from aqueous solutions by akaganeite, *J. Hazard. Mater.*, 2008, **160**, 388–395.
3 J. Kim and C. P. Grey, ^2H and ^7Li Solid-State MAS NMR Study of Local Environments and Lithium Adsorption on the Iron(III) Oxyhydroxide, Akaganeite (β-FeOOH), *Chem. Mater.*, 2010, **22**, 5453–5462.
4 T. Ishikawa, R. Katoh, A. Yasukawa, K. Kandori, T. Nakayama and F. Yuse, Influences of metal ions on the formation of beta-FeOOH particles, *Corros. Sci.*, 2001, **43**, 1727–1738.
5 K. Fominykh, D. Böhm, S. Zhang, A. Folger, M. Döblinger, T. Bein, C. Scheu and D. Fattakhova-Rohlfing, Nonagglomerated Iron Oxyhydroxide Akaganeite Nanocrystals Incorporating Extraordinary High Amounts of Different Dopants, *Chem. Mater.*, 2017, **29**, 7223–7233.
6 X. Guo, Z. Wu, M. He, X. Meng, X. Jin, N. Qiu and J. Zhang, Adsorption of antimony onto iron oxyhydroxides: Adsorption behaviour and surface structure, *J. Hazard. Mater.*, 2014, **276**, 339–345.
7 Y. X. Zhang and Y. Jia, A facile solution approach for the synthesis of akaganéite (β-FeOOH) nanorods and their ion-exchange mechanism toward As(V) ions, *Appl. Surf. Sci.*, 2014, **290**, 102–106.
8 F. Kolbe, H. Weiss, P. Morgenstern, R. Wennrich, W. Lorenz, K. Schurk, H. Stanjek and B. Daus, Sorption of aqueous antimony and arsenic species onto akaganeite, *J. Colloid Interface Sci.*, 2011, **357**, 460–465.
9 S. Yusan and S. A. Erenturk, Adsorption equilibrium and kinetics of U(VI) on beta type of akaganeite, *Desalination*, 2010, **263**, 233–239.
10 E. A. Deliyanni, E. N. Peleka and K. A. Matis, Removal of zinc ion from water by sorption onto iron-based nanoadsorbent, *J. Hazard. Mater.*, 2007, **141**, 176–184.
11 N. K. Lazaridis, D. N. Bakoyannakis and E. A. Deliyanni, Chromium(VI) sorptive removal from aqueous solutions by nanocrystalline akaganeite, *Chemosphere*, 2005, **58**, 65–73.
12 E. A. Deliyanni and K. A. Matis, Sorption of Cd ions onto akaganeite-type nanocrystals, *Sep. Purif. Technol.*, 2005, **45**, 96–102.
13 F. Parvin, S. Y. Rikta and S. M. Tareq, Application of Nanomaterials for the Removal of Heavy Metal from Wastewater, in *Nanotechnology in Water and Wastewater Treatment*, ed. A. Ahsan and A. F. Ismail, Elsevier, 2019, vol. 137–157, ISBN 9780128139028.
14 E. A. Deliyanni, G. Z. Kyzas and K. A. Matis, Inorganic nanoadsorbent: Akaganeite in wastewater treatment, in *Composite Nanoadsorbents*, ed. G. Z. Kyzas and A. C. Mitropoulos, Elsevier, 2019, vol. 337–358, ISBN 9780128141328.
15 A. E. Tufo, A. L. Larralde, J. Villarroel-Rocha, K. Sapag and E. E. Sileo, Synthesis and characterization of pure and Al-substituted akaganeites and evaluation of their performance to adsorb As(V), *J. Environ. Chem. Eng.*, 2018, **6**, 7044–7053.
16 X. Sun, C. Hu, X. Hu, J. Qu and M. Yang, Characterization and adsorption performance of Zr-doped akaganeite for

efficient arsenic removal, *J. Chem. Technol. Biotechnol.*, 2013, **88**, 629–635.

17 D. K. L. Harijan and V. Chandra, Akaganeite nanorods decorated graphene oxide sheets for removal and recovery of aqueous phosphate, *J. Water Process Eng.*, 2017, **19**, 120–125.

18 E. A. Deliyanni, E. N. Peleka and K. A. Matis, Effect of cationic surfactant on the adsorption of arsenites onto akaganeite nanocrystals, *Sep. Sci. Technol.*, 2007, **42**, 993–1012.

19 E. A. Deliyanni, L. Nalbandian and K. A. Matis, Adsorptive removal of arsenites by nanocrystalline hybrid surfactant-akaganeite sorbent, *J. Colloid Interface Sci.*, 2006, **302**, 458–466.

20 V. Villacorta, K. E. García, J.-M. Greneche and C. A. Barrero, Influences of As(V), Sb(III), and Hg(II) ions on the nucleation and growth of akaganeite, *CrystEngComm*, 2019, **46**, 7155–7165.

21 J. P. Gustafsson, *Visual MINTEQ 3.1*, 2013.

22 K. Ehlert, C. Mikutta, Y. Jin and R. Kretzschmar, Mineralogical Controls on the Bioaccessibility of Arsenic in Fe(III)-As(V) coprecipitates, *Environ. Sci. Technol.*, 2018, **52**, 616–627.

23 G. K. Schweitzer and L. L. Pesterfield, *The aqueous Chemistry of the Elements*, Oxford University Press, Inc., New York, 2010.

24 L. Li and R. Stanforth, Distinguishing Adsorption and Surface Precipitation of Phosphate on Goethite (α-FeOOH), *J. Colloid Interface Sci.*, 2000, **230**, 12–21.

25 S. Goldberg, Surface Complexation Modeling, *Reference Module in Earth Systems and Environmental Sciences*, 2013, DOI: 10.1016/B978-0-12-409548-9.05311-2.

26 X. Yang, Y. Wan, Y. Zheng, F. He, Z. Yu, J. Huang, H. Wang, Y. S. Ok, Y. Jiang and B. Gao, Surface functional groups of carbon-based adsorbents and their roles in the removal of heavy metals from aqueous solutions: A critical review, *Chem. Eng. J.*, 2019, **366**, 608–621.

27 A. Ler and R. Stanforth, Evidence for Surface precipitation of phosphate on goethite, *Environ. Sci. Technol.*, 2003, **37**, 2694–2700.

28 R. M. Cornell and U. Schwertmann, *The Iron Oxides. Structure, Properties, Reactions, Occurrences and Uses*, Wiley-VCH Verlag GmbH & Co. KGaA, 2nd edn, 2003.

29 L. Largitte and R. Pasquier, A review of the kinetics adsorption models and their application to the adsorption of lead by an activated carbon, *Chem. Eng. Res. Des.*, 2016, **109**, 495–504.

30 J. P. Jolivet, *Metal Oxide Chemistry and Synthesis. From solution to solid stated*, John Wiley & Sons Inc, 1st edn, 1994.

31 E. A. Deliyanni, D. N. Bakoyannakis, A. I. Zouboulis and K. A. Matis, Sorption of As(V) ions by akaganéite-type nanocrystals, *Chemosphere*, 2003, **50**, 155–163.

32 X. Song and J. F. Boily, Surface Hydroxyl Identity and Reactivity in Akaganéite, *J. Phys. Chem. C*, 2011, **115**, 17036–17045.

